Available online at www.sciencedirect.com

ScienceDirect

Trans. Nonferrous Met. Soc. China 26(2016) 712−721

Transactions of Nonferrous Metals Society of China

www.tnmsc.cn

Plastic flow behavior of superalloy GH696 during hot deformation

Zhao-hua XU, Miao-quan LI, Hong LI

School of Materials Science and Engineering, Northwestern Polytechnical University, Xi'an 710072, China

Received 23 March 2015; accepted 20 October 2015

Abstract: In order to investigate the hot deformation behavior of superalloy GH696, isothermal compression experiments were carried out at deformation temperatures of 880−1120 °C and strain rates of 0.01−10 s^{-1}. And the deformation amount of all the samples was 50%. The strain rate sensitivity exponent (m) and strain hardening exponent (n) under different deformation conditions were calculated, meanwhile the effects of the processing parameters on the values of m and n were analyzed. The results show that the flow stress increases with the increase of strain rate and the decrease of deformation temperature. The value of m increases with the increase of deformation temperature and decreases with the increase of strain rate, while the value of n decreases with the increase of deformation temperature. A novel flow stress model during hot deformation of superalloy GH696 was also established. And the calculated flow stress of the alloy is in good agreement with the experimental one.

Key words: superalloy GH696; flow stress; deformation behavior; strain rate sensitivity exponent; strain hardening exponent; flow stress model

1 Introduction

Superalloy GH696 is an aging hardening Fe-based superalloy with excellent low thermal expansion property at high working temperatures. Besides its good corrosion resistance, high strength at elevated temperatures and good thermostablity, it also possesses heat resisting property up to 700 °C. Superalloy GH696 containing 3% Ti and 0.5% Al (mass fraction) is strengthened not only by the precipitation of γ' phase (Ni_3AlTi) in matrix by following aging after solution treatment, but also by the grain boundary hardening of B and the solid solution hardening of Mo; the low cost and excellent working properties result in its widely application in gas turbine as high temperature attaching parts and spring [1−3]. Due to poor working conditions, such as high temperature, corrosive atmosphere, high altering stress and creep loads, superalloy components with favorable microstructure and fine grains must be guaranteed by controlling the forging process. However, the workability of superalloys during hot deformation is poor due to the large content of alloying elements.

So, a large number of investigations were done on the isothermal deformation behavior of superalloys. CAI et al [4] investigated the hot deformation behavior of superalloy GH696, in which a model for peak stress and processing maps were achieved and the apparent activation energy for deformation was calculated to be about 499 kJ/mol. DEHGHAN et al [5] showed that the flow stress−strain curves of superalloy A286 were the dynamic recrystallization type; however, some reflected the change between continuous and discontinuous recrystallization with the change of strain rate. CICCO et al [6] established a model for steady state deformation of superalloy A286 based on the theory of thermally activated glide. GAO et al [7] investigated the high temperature deformation of an Fe-based low nickel superalloy. The results showed that dynamic recovery was the dominating softening mechanism during hot deformation of this alloy. Furthermore, the plastic deformation behavior and flow stress model for superalloy GH4169 during hot deformation were presented [8,9]. MEDEIROS et al [10] focused on the hot deformation behavior of cast and solution-treated Inconel 718. Researchers [11−13] established the peak flow stress of superalloys as a function of deformation temperature and strain rate. WU et al [14], ZHANG et al [15] and LIN et al [16] established the flow stress models reflecting the effect of deformation temperature, strain rate and strain on flow stress. However, these researches mainly focused on Ni-based superalloy. Few

Corresponding author: Miao-quan LI; Tel: +86-29-88460328; Fax: +86-29-88492642; E-mail: honeymli@nwpu.edu.cn
DOI: 10.1016/S1003-6326(16)64161-4

researches were done on the hot deformation behavior of Fe-based superalloy.

It is well known that the hot deformation behavior of materials strongly depends on the processing parameters such as deformation temperature, strain rate and strain [17]. ABBASI et al [18] found that the strain rate sensitivity exponent of superalloy Fe−29Ni−17Co increased with the increase of deformation temperature below 1100 ℃. SALEHI et al [19] noted that the strain rate sensitivity exponent of superalloy A286 increased with the increase of deformation temperature. In addition, the strain hardening exponent reflects the work-hardening effect of material and relates to the uniform plastic strain [20]. However, few efforts have been made to investigate the strain hardening exponent of superalloys during hot deformation. WANG et al [17] studied the effect of δ phase on the deformation behavior of superalloy GH4169, which showed that the strain hardening exponent was significantly affected by the deformation parameters, especially the strain; and the existence of δ phase resulted in the decrease of n values. However, these researches did not analyze the effects of deformation parameters on the strain rate sensitivity exponent and strain hardening exponent in depth.

The objective of this study was to investigate the plastic flow behavior of Fe-based superalloy GH696 during hot deformation. The strain rate sensitivity exponent and strain hardening exponent of superalloy GH696 during isothermal compression under different deformation conditions were calculated. Meanwhile, a novel model considering the effect of strain on flow stress of superalloy GH696 during isothermal compression was also established.

2 Experimental

2.1 Material

The chemical composition of as-received superalloy GH696 is shown in Table 1. The material was supplied as hot-rolled state. The optical microstructure consisting of equiaxed austenite grains with a diameter of about 30 μm is shown in Fig. 1. The cylindrical specimens for isothermal compression are manufactured from the as-received superalloy GH696 bar with a diameter of 8 mm and a height of 12 mm.

2.2 Isothermal compression

Isothermal compression tests of superalloy GH696 were conducted on a Gleeble−3500 simulator at deformation temperatures ranging from 880 to 1120 ℃ with an interval of 30 ℃, strain rates of 0.01, 0.1, 1 and 10 s^{-1}. And the deformation amount is 50%. Prior to compression, the specimens were heated at a heating rate of 10 ℃/s and held for 5 min at the setting deformation

Table 1 Chemical composition of as-received superalloy GH696 (mass fraction, %)

Ni	Cr	Mo	Ti	Al	Mn	Fe
21.0−25.0	10.0−12.5	1.0−1.6	2.6−3.2	≤0.80	≤0.6	Bal.

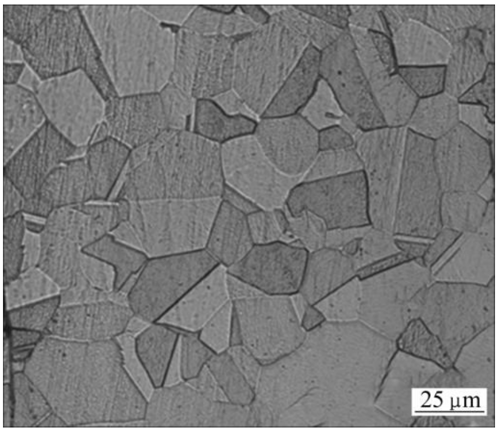

Fig. 1 Optical micrograph of as-received superalloy GH696

temperature to ensure the uniform temperature distribution in specimens before compression. After the compression, the specimens were quenched in water. Then, the compressed specimens were sectioned parallel to the compression axis and prepared to observe the microstructure. The chemical etch was 50 mL HCl + 50 mL CH_3CH_2OH + 15 g $FeCl_3$. And the metallographic observation was carried out on Leica DMI 3000 M optical microscope (OM).

3 Results and discussion

3.1 Flow stress

Figure 2 shows the variation of flow stress with strain at strain rates ranging from 0.01 to 10 s^{-1} and deformation temperatures ranging from 880 to 1120 ℃. As seen from Fig. 2, the flow stress is evidently affected by both deformation temperature and strain rate. In general, the flow stress of superalloy GH696 during the isothermal compression increases with the increase of strain rate and decreases with the increase of deformation temperature.

In terms of the dynamic softening mechanism during hot deformation, the flow stress−strain curves can be divided into two types, namely dynamic recovery type and dynamic recrystallization type [21]. As seen from Fig. 2, the flow stress−strain curves of superalloy GH696 include two types. The flow stress−strain curves of superalloy GH696 are characterized with the occurrence of dynamic recrystallization at high deformation temperatures and low strain rates and dynamic recovery at low deformation temperatures and high strain rates. As seen from Fig. 2, the flow stress of superalloy GH696

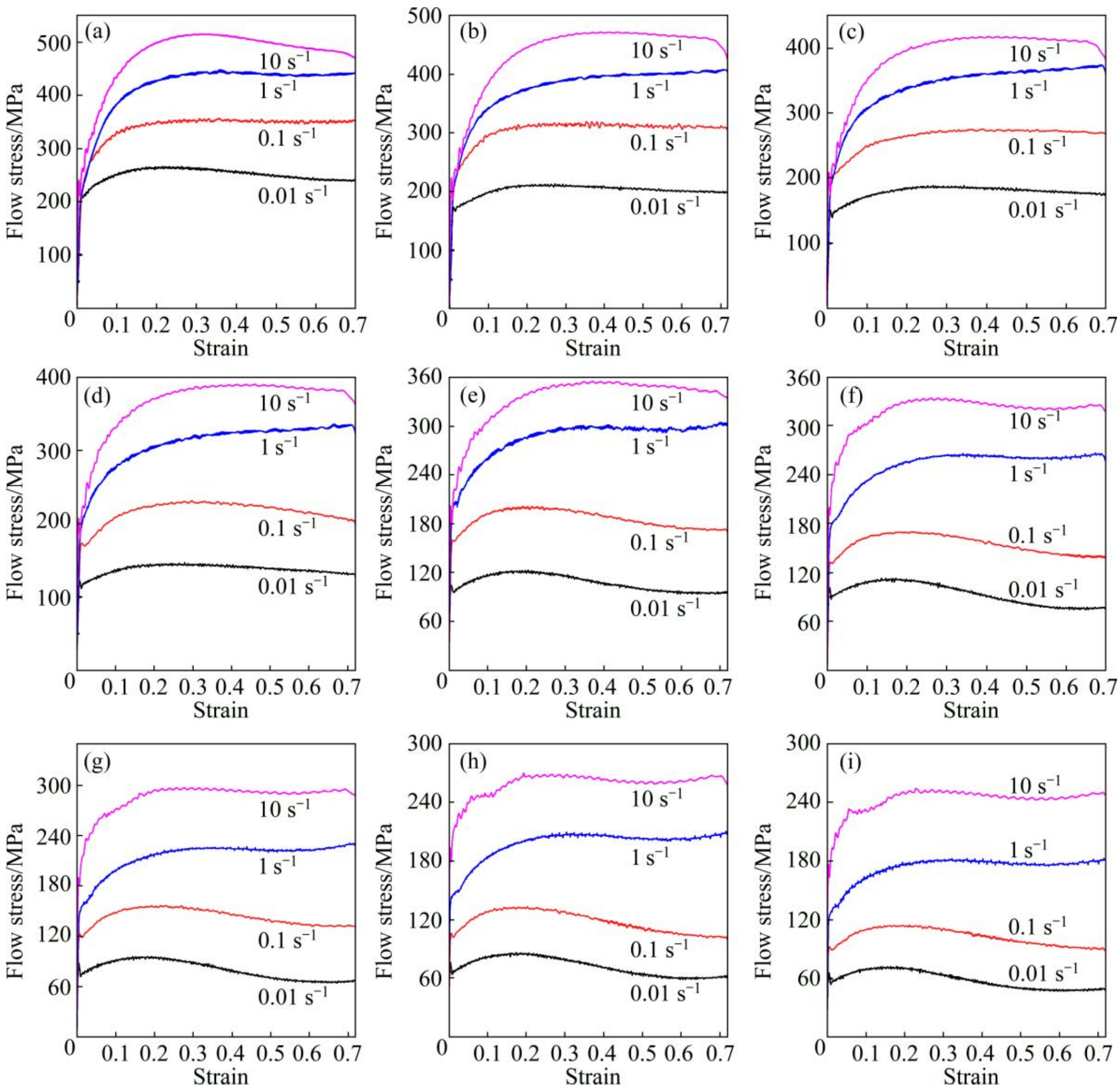

Fig. 2 Flow stress−strain curves of isothermally compressed superalloy GH696 at different strain rates: (a) 880 ℃; (b) 910 ℃; (c) 940 ℃; (d) 970 ℃; (e) 1000 ℃; (f) 1030 ℃; (g) 1060 ℃; (h) 1090 ℃; (i) 1120 ℃

presents a sharp increase at the beginning of compression and then reaches a peak, which can be explained as the fact that the significant generation, multiplication and intersection of dislocation with the increase of strain lead to large work-hardening effect. Meanwhile, dynamic recovery in this stage is not enough to eliminate the work-hardening effect, resulting in a quick increase of flow stress. As the dynamic recovery of superalloy GH696 continues and the dynamic recrystallization begins, the increase of the flow stress slows down until it reaches the peak. After the peak, the flow stress−strain curves of superalloy GH696 have a slight decrease with the increase of strain at high deformation temperatures and low strain rates. On one hand, that is because high deformation temperatures can provide more energy for the motion of dislocation and vacancy, which facilitates dynamic recovery and dynamic recrystallization; on the other hand, there will be longer time for dynamic softening at lower strain rates, which leads to the decrease of flow stress. However, the flow stress of superalloy GH696 at low deformation temperature and high strain rate reaches a steady state after the peak. Besides, the peak flow stress of superalloy GH696 does not appear at a strain rate of 1 s^{-1} and the deformation temperatures ranging from 910 to 970 ℃, which implies that the work-hardening effect is the dominant effect throughout the whole compression tests under these compression conditions.

3.2 Strain rate sensitivity exponent

Strain rate sensitivity exponent (*m*) represents the capacity of material resisting necking and affects the stability of deformation [17]. Generally, the higher the strain rate sensitivity exponent is, the better the workability of material during hot deformation is. The strain rate sensitivity exponent of superalloy GH696 at a certain strain and deformation temperature can be calculated by the following equation:

$$m=\left.\frac{\partial \ln \sigma}{\partial \ln \dot{\varepsilon}}\right|_{\varepsilon,T} \tag{1}$$

where σ is the flow stress (MPa), $\dot{\varepsilon}$ is the strain rate (s^{-1}), ε is the strain, and T is the deformation temperature (K).

Based on the experimental data, the relationship between $\ln \sigma$ and $\ln\dot{\varepsilon}$ can be approximately expressed by three order polymonimal as shown in Eq. (2). So, the strain rate sensitivity exponent can be calculated easily by Eq. (2).

$$\ln \sigma = a + b\ln\dot{\varepsilon} + c(\ln\dot{\varepsilon})^2 + d(\ln\dot{\varepsilon})^3 \tag{2}$$

where a, b, c and d are material constants.

The variation of the calculated strain rate sensitivity exponent with the deformation temperature at different strains is shown in Fig. 3. As seen from Fig. 3, the strain rate sensitivity exponent increases with the rise of deformation temperature. That is because the mobility of dislocation and grain boundaries is elevated with the increase of deformation temperature, which accelerates the dynamic recovery and recrystallization. Figure 3 also shows that the strain rate sensitivity exponent is evidently affected by the strain rate. The lower the strain rate is, the larger the strain rate sensitivity exponent is. Because lower strain rate leads to longer deformation time, there will be more time for dynamic softening which decreases the deformation resistance. As a result, the workability of superalloy GH696 is enhanced with the decrease of strain rate.

Besides, the strain rate sensitivity exponent at a strain rate of 0.01 s^{-1} fluctuates horizontally with the increase of deformation temperatures above 1000 ℃ because the dynamic recrystallization has already completed at these deformation temperatures, as shown in Fig. 4, and the grain size at 1090 ℃ is just about 35 μm. So, the effect of the deformation temperature on the strain rate sensitivity exponent is slight. Furthermore, the strain rate sensitivity exponent fluctuates at a very low level at deformation temperatures below 1000 ℃ and a strain rate of 10 s^{-1}. On one hand, that is because the dislocation multiplies rapidly at high strain rates; on the other hand, the softening effect caused by deformation temperature at low deformation temperature is not large enough to increase the strain rate sensitivity exponent greatly.

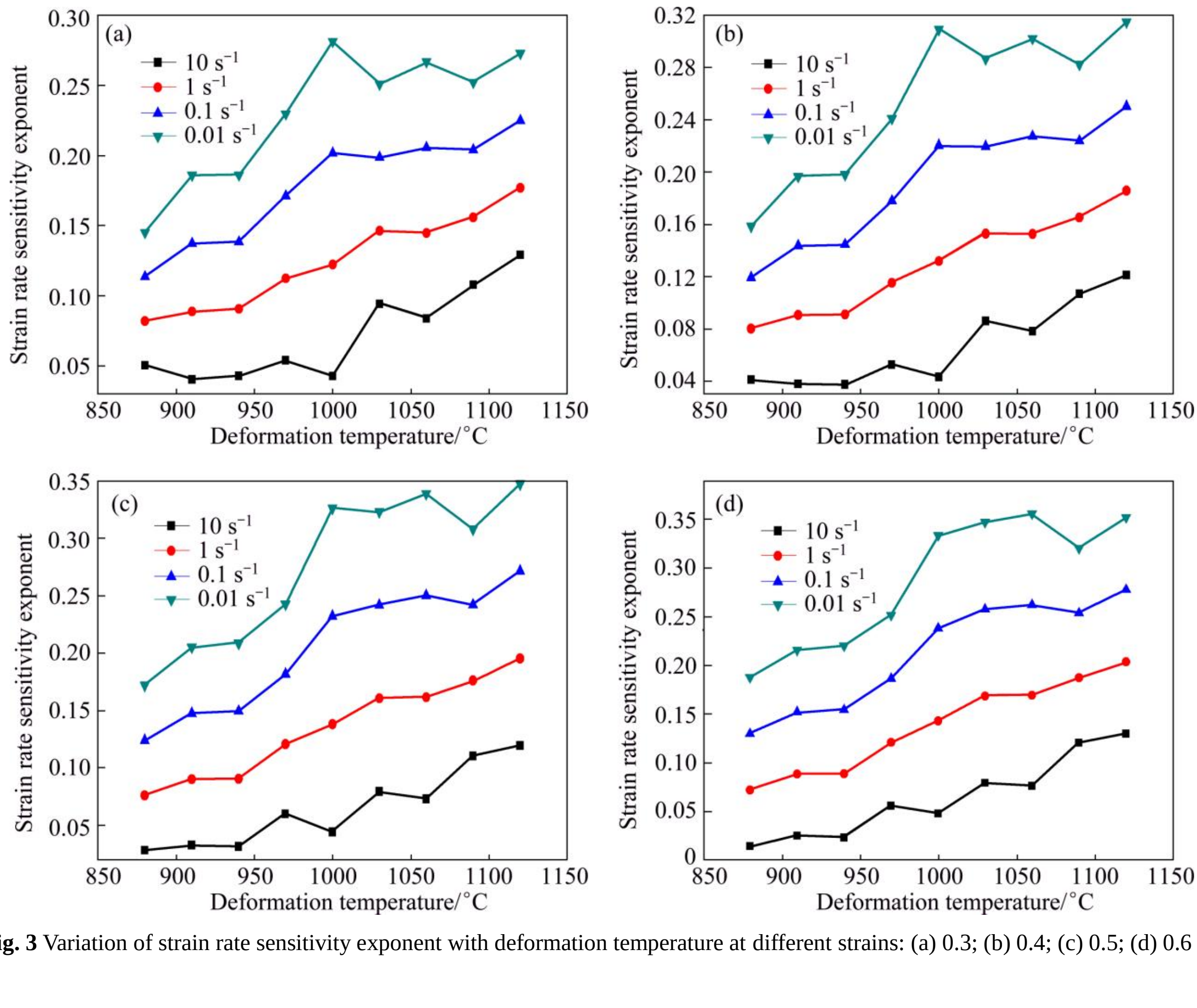

Fig. 3 Variation of strain rate sensitivity exponent with deformation temperature at different strains: (a) 0.3; (b) 0.4; (c) 0.5; (d) 0.6

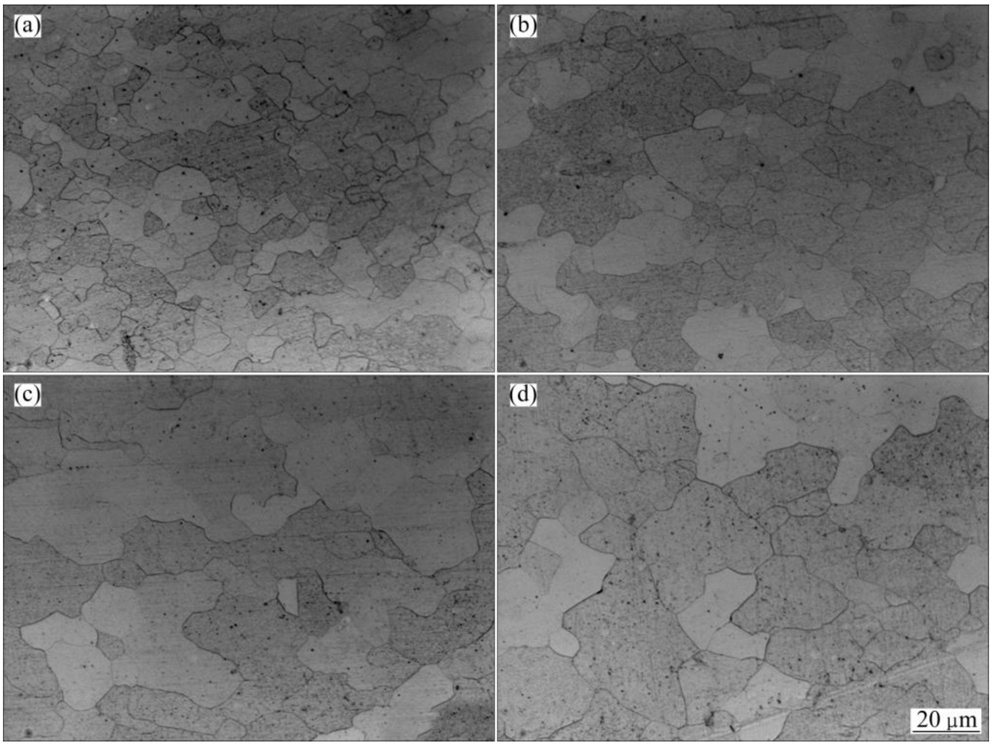

Fig. 4 Microstructures of isothermally compressed superalloy GH696 at strain rate of 0.01 s^{-1}, deformation amount of 50% and different deformation temperatures: (a) 1000 °C; (b) 1030 °C; (c) 1060 °C; (d) 1090 °C

3.3 Strain hardening exponent

The strain hardening exponent (n) results from a balance between the work-hardening effect and the softening effect, which mainly depends on strain and deformation time [17,22]. And the strain hardening exponent under different deformation conditions can be calculated with the following equation:

$$n = \left.\frac{\partial \ln \sigma}{\partial \ln \varepsilon}\right|_{\dot{\varepsilon},T} \tag{3}$$

Based on the experimental data, the relationship between ln σ and ln ε can be approximately expressed by five order polymonimal as shown in Eq. (4). So, the strain hardening exponent can be calculated easily by Eq. (4):

$$\ln\sigma = a + b\ln\varepsilon + c(\ln\varepsilon)^2 + d(\ln\varepsilon)^3 + e(\ln\varepsilon)^4 + f(\ln\varepsilon)^5 \tag{4}$$

where a, b, c, d, e and f are material constants.

The variation of the calculated strain hardening exponent (n) with the deformation temperature at different strains is shown in Fig. 5. As seen from Fig. 5, the strain hardening exponent has a slight increase with the increase of deformation temperature up to 950 °C. It is well known that the second-phase particles γ'(Ni_3AlTi) in superalloy GH696 completely dissolve into the matrix at the deformation temperatures about 950 °C [23]. Then, the lower the deformation temperature is, the more the strengthening phases in matrix are, which leads to higher deformation resistance. As a result, energy storage for deformation in superalloy increases, promoting the dynamic recovery and dynamic recrystallization. Therefore, the softening effect at lower deformation temperatures is more powerful than that at higher deformation temperatures, which finally leads to larger strain hardening exponent at high deformation temperatures. After the slight increase, the strain hardening exponent decreases with the rise of deformation temperature and then fluctuates at strain rates of 10 and 1 s^{-1}. That is because large strain rate can cause intense multiplication of dislocation and short deformation time, as a result, little effect on grain size and strain hardening exponent is caused by increasing deformation temperature as shown in Fig. 6. In addition, the strain hardening exponent quickly decreases at strain rates of 0.1 and 0.01 s^{-1} and deformation temperatures above 970 °C as the amount of strengthening phases decreases with the increase of deformation temperature. Besides, nearly full dynamic recrystallization occurs at deformation temperatures about 970 °C, which enhances the softening effect, leading to the sharp decrease in strain hardening exponent. The strain hardening exponent at a strain rate of 0.01 s^{-1} and deformation temperatures above 1030 °C begins to increase as shown in Figs. 5(c) and (d) because the deformation time is prolonged at lower strain rates and higher strains. Based

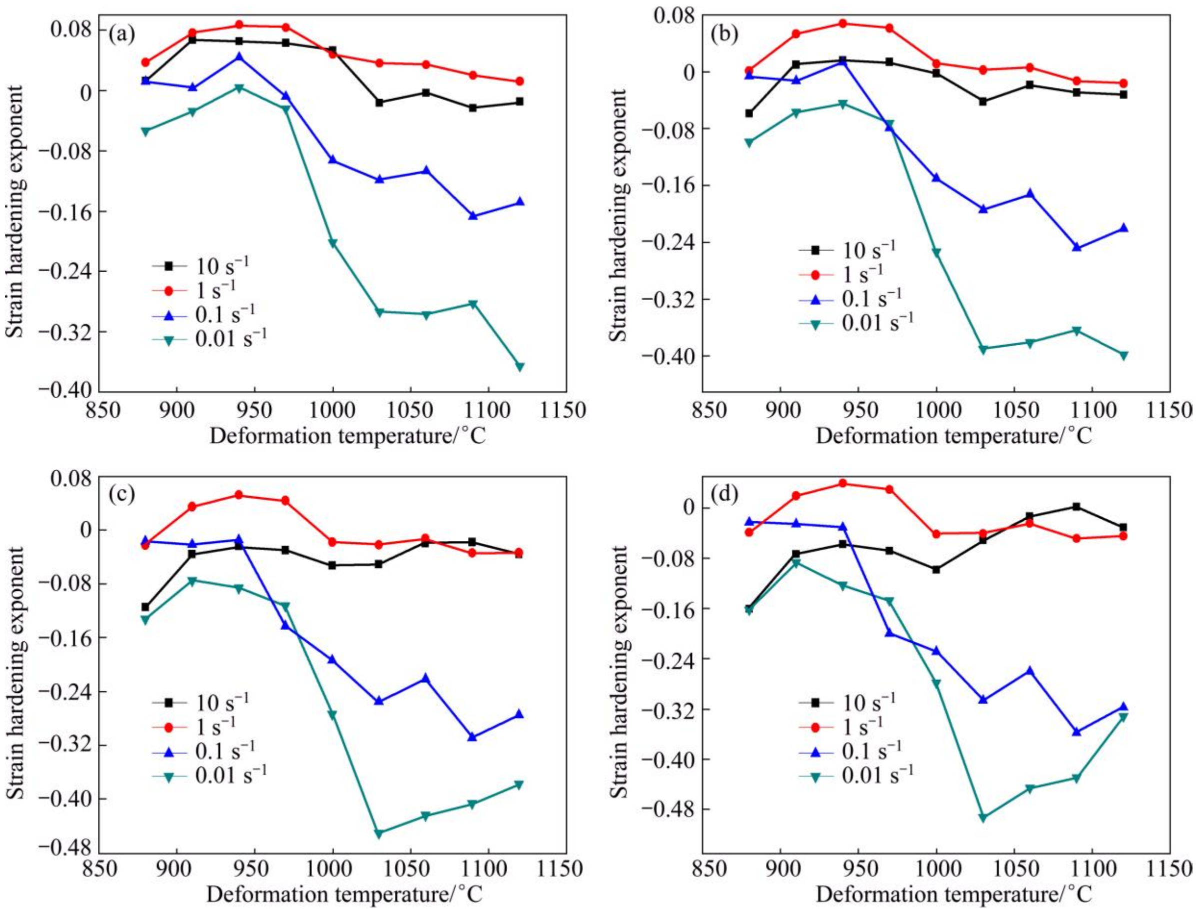

Fig. 5 Variation of strain hardening exponent with deformation temperature at different strains: (a) 0.3; (b) 0.4; (c) 0.5; (d) 0.6

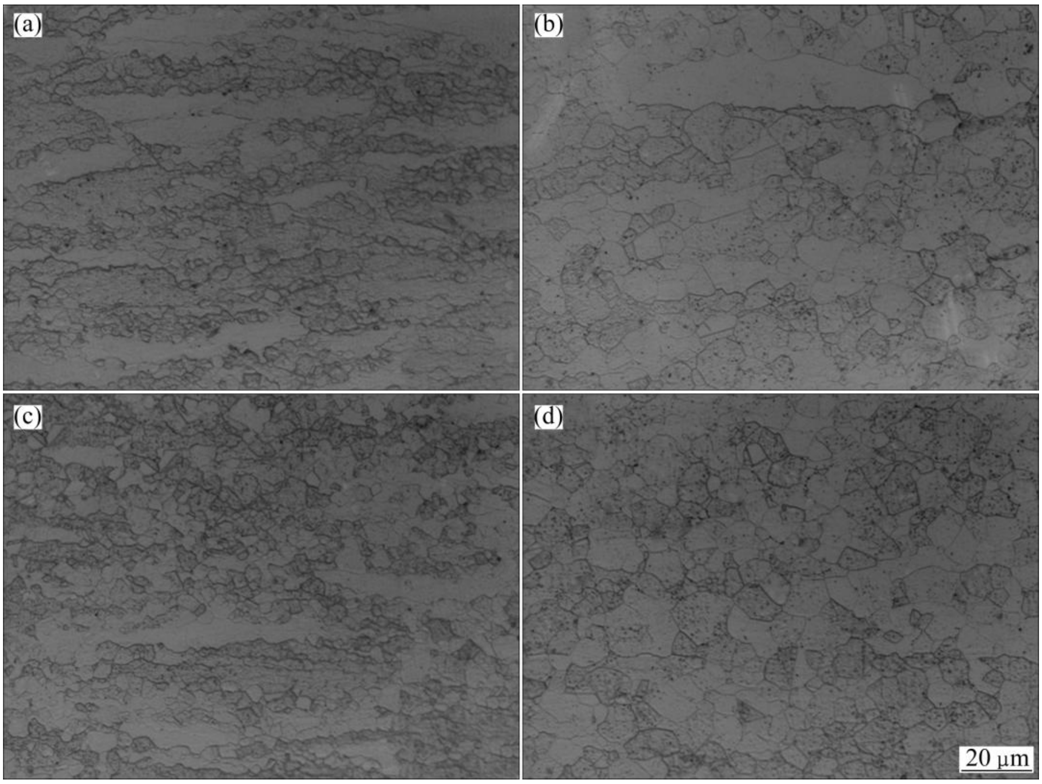

Fig. 6 Microstructures of isothermally compressed superalloy GH696 under different deformation conditions: (a) 1030 ℃, 1 s^{-1}; (b) 1090 ℃, 1 s^{-1}; (c) 1030 ℃, 10 s^{-1}; (d) 1090 ℃, 10 s^{-1}

on the above analysis, the growth of recrystallized grains of superalloy GH696 after completing dynamic recrystallization leads to the sharp decrease of grains for deformation, as shown in Figs. 4(b)−(d). Consequently, the strain hardening exponent becomes larger. Besides, as shown in Fig. 5, the strain hardening exponents at strain rates of 0.1 and 0.01 s^{-1} are negative at all deformation temperatures, which means that the softening effect is stronger than the work-hardening effect at strains of 0.3−0.6.

3.4 Flow stress model

The constitutive model describing the dependence of the flow stress on the strain rate and deformation temperature during hot deformation is obtained by using the phenomenological approach in the following equation [24].

$$\dot{\varepsilon} = A[\sinh(\alpha\sigma)]^{n_1} \exp\left(-\frac{Q}{RT}\right) \tag{5}$$

where $\dot{\varepsilon}$ is the strain rate (s^{-1}), σ is the flow stress (MPa), A and α are material constants, n_1 is the stress exponent, Q is the apparent activation energy for deformation (kJ/mol), R is the mole gas constant (J/(mol·K)), and T is the deformation temperature (K).

The effect of the deformation temperature and strain rate on the deformation behavior can also be substituted by Zener−Hollomon parameter (Z-parameter) in the following form:

$$Z = \dot{\varepsilon} \exp\left(\frac{Q}{RT}\right) \tag{6}$$

Taking the effect of strain on the flow stress into consideration in Eq. (5), we will get

$$f(\varepsilon)\dot{\varepsilon} = A[\sinh(\alpha\sigma)]^{n_1} \exp\left(-\frac{Q}{RT}\right) \tag{7}$$

Taking the natural logarithm of Eq. (7), the model is rewritten as follows:

$$\ln[\sinh(\alpha\sigma)] = A_1 + A_2 \ln Z + \ln f(\varepsilon) \tag{8}$$

where A_1 and A_2 are material constants.

The relationship between ln[sinh($\alpha\sigma$)] and ln ε in Fig. 7 shows that ln[sinh($\alpha\sigma$)] can be expressed by three order polynomial of ln ε. In other words, ln $f(\varepsilon)$ can be expressed by three order polynominal of ln ε. So, Eq. (8) can also be written as

$$\ln[\sinh(\alpha\sigma)] = C_1 + C_2 \ln Z + C_3 \ln\varepsilon + C_4 (\ln\varepsilon)^2 + C_5 (\ln\varepsilon)^3 \tag{9}$$

where C_1, C_2, C_3, C_4 and C_5 are material constants.

In order to improve the precision of Eq. (9), the equation can be expressed as Eq. (10). So, Eq. (10) is the flow stress model proposed for superalloy GH696.

$$\ln[\sinh(\alpha\sigma)] = B_0 + B_1 \ln Z + B_2 (\ln Z)^2 + B_3 \ln\varepsilon + B_4 (\ln\varepsilon)^2 + B_5 (\ln\varepsilon)^3 \tag{10}$$

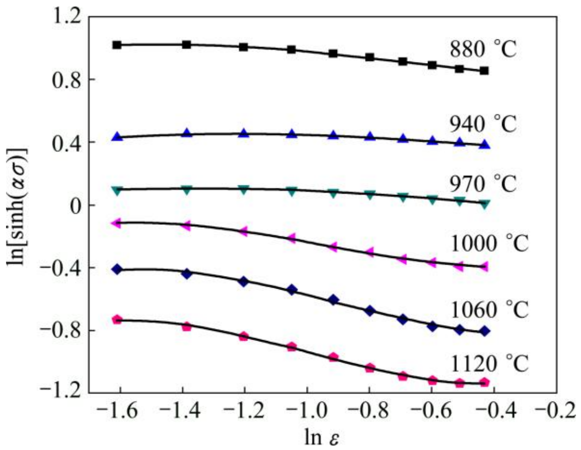

Fig. 7 Relationship between ln[sinh($\alpha\sigma$)] and ln ε at strain rate of 0.01s^{-1}

where B_0, B_1, B_2, B_3, B_4 and B_5 are material constants.

Taking the natural logarithm of Eq. (5), the model is rewritten as follows:

$$\ln[\sinh(\alpha\sigma)] = -\frac{1}{n_1}\ln A + \frac{Q}{n_1 RT} + \frac{\ln\dot{\varepsilon}}{n_1} \tag{11}$$

In order to calculate the values of A, n_1 and Q, seven values of α are given, and the corresponding residual sum of squares can be calculated by fitting the experimental data. It is well known that the α-value minimizing the residual sum of squares is the optimum [25]. As seen from Fig. 8, the optimum α-value is 7.21 kPa^{-1} at a strain of 0.5.

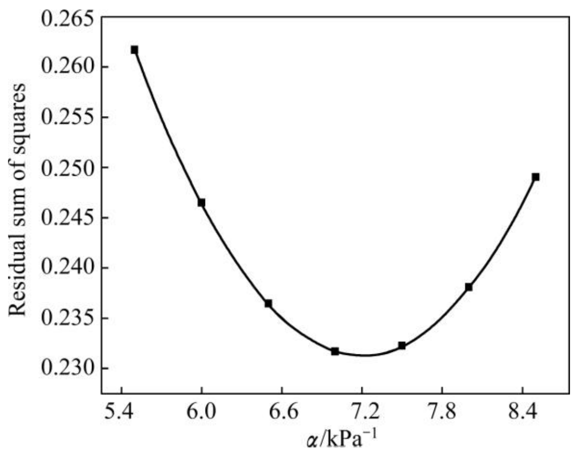

Fig. 8 Variation of residual sum of squares with α at strain of 0.5

Fixing the deformation temperature, the stress exponent (n_1) can be calculated by the following equation:

$$n_1 = \left.\frac{\partial \ln\dot{\varepsilon}}{\partial \ln[\sinh(\alpha\sigma)]}\right|_T \tag{12}$$

As a result, the value of n_1 at a strain of 0.5 is 3.507, which is equal to the reciprocal of the average value of the slopes of the lines in Fig. 9(a). And the average correlation coefficient of the lines is greater than 0.98.

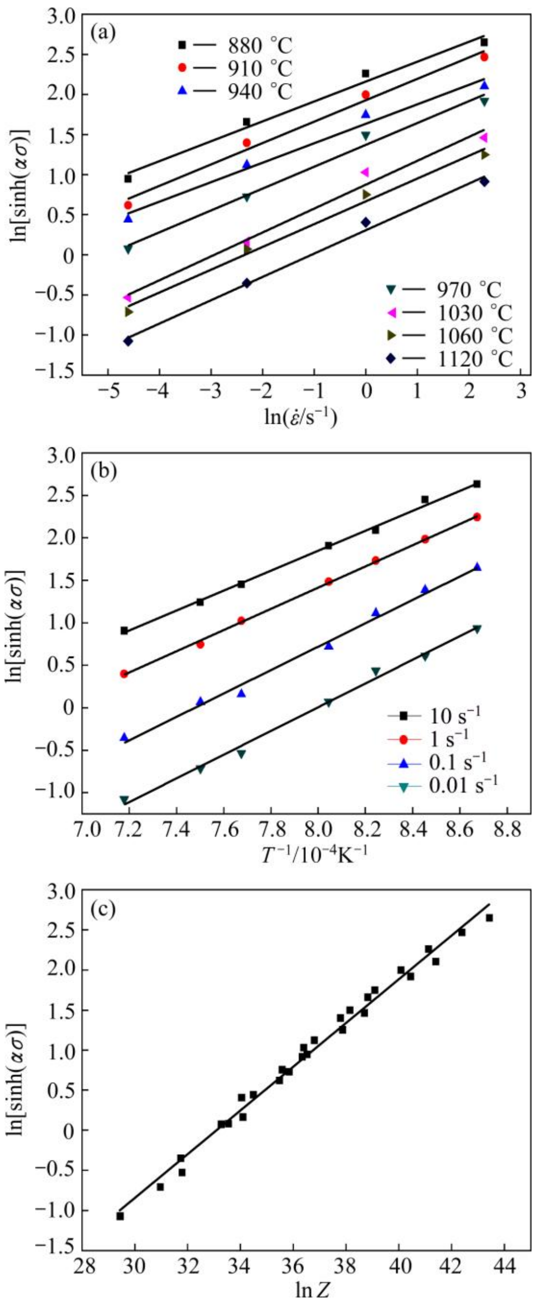

Fig. 9 Relationship among flow stress and strain rate (a), deformation temperature (b) and Zener−Hollomon parameter (c)

Fixing the strain rate, the value of Q is calculated by the following equation:

$$Q = n_1 R \left. \frac{\partial \ln[\sinh(\alpha\sigma)]}{\partial(1/T)} \right|_{\dot{\varepsilon}} \tag{13}$$

Apparently, the average slope of the lines in Fig. 9(b) is equal to the value of $Q/(10^4 n_1 R)$, then the value of Q at a strain of 0.5 is calculated to be 395.751 kJ/mol. And the average correlation coefficient of the lines is greater than 0.99.

Applying the regression method, the relationship between the flow stress and the Z-parameter of superalloy GH696 during hot deformation is shown in Fig. 9(c). As seen from Fig. 9(c), the experimental data fit well with the hyperbolic law, and the value of A at a strain of 0.5 is 1.99×10^{14} s^{-1}.

Repeating the above-presented procedures, the values of α, n_1, Q and A at strains of 0.20−0.60 with an interval of 0.05 are calculated and shown in Table 2. The calculated apparent activation energy for deformation of superalloy GH696 is in the range of 389.524−410.236 kJ/mol, and the average value of Q is 399.9 kJ/mol. The average value of α is 6.62 kPa^{-1}.

Table 2 Values of α, n_1, Q and A at strains of 0.20−0.60

Strain	α/kPa^{-1}	n_1	Q/(kJ·mol^{-1})	A/s^{-1}
0.20	5.67	4.740	410.236	1.479×10^{15}
0.25	5.89	4.465	408.073	9.881×10^{14}
0.30	6.19	4.182	403.752	5.462×10^{14}
0.35	6.50	3.951	401.699	3.898×10^{14}
0.40	6.82	3.743	399.081	2.765×10^{14}
0.45	7.12	3.581	398.159	2.353×10^{14}
0.50	7.21	3.507	395.751	1.990×10^{14}
0.55	7.21	3.480	392.839	1.642×10^{14}
0.60	6.93	3.545	389.524	1.529×10^{14}

Applying the multiple linear regression method, the flow stress model of superalloy GH696 during hot deformation is as follows:

$$\begin{aligned}\sigma = {} & 151.0574\,\mathrm{arsinh}\{\exp[-7.6188+0.1818\ln Z+\\ & 0.0013(\ln Z)^2+0.0598\ln\varepsilon+0.3742(\ln\varepsilon)^2+\\ & 0.1617(\ln\varepsilon)^3]\},\quad \dot{\varepsilon}\le 0.1\ \mathrm{s}^{-1}\end{aligned} \tag{14a}$$

$$\begin{aligned}\sigma = {} & 151.0574\,\mathrm{arsinh}\{\exp[-9.8462+0.3548\ln Z-\\ & 0.0016(\ln Z)^2+0.1488\ln\varepsilon+0.2874(\ln\varepsilon)^2+\\ & 0.1418(\ln\varepsilon)^3]\},\quad \dot{\varepsilon}>0.1\ \mathrm{s}^{-1}\end{aligned} \tag{14b}$$

where $Z=\dot{\varepsilon}\exp\left(\dfrac{399900}{RT}\right)$.

3.5 Verification of model

In order to verify the flow stress model of superalloy GH696 during hot deformation, a comparison of the calculated flow stress with the experimental results at deformation temperatures of 1000 ℃ and 1090 ℃ was carried out. The results are shown in Fig. 10. As seen from Fig. 10, the calculated results are in good agreement with the experimental results. In order to further confirm the prediction accuracy of the developed constitutive model, the average absolute relative errors (E) are also calculated by Eq. (15):

$$E=\frac{1}{N}\sum_{i=1}^{N}\left|\frac{X_i-Y_i}{X_i}\right|\times100\% \tag{15}$$

where $X_{\rm i}$ is the measured flow stress (MPa), $Y_{\rm i}$ is the predicted flow stress (MPa), and N is the number of stress−strain samples.

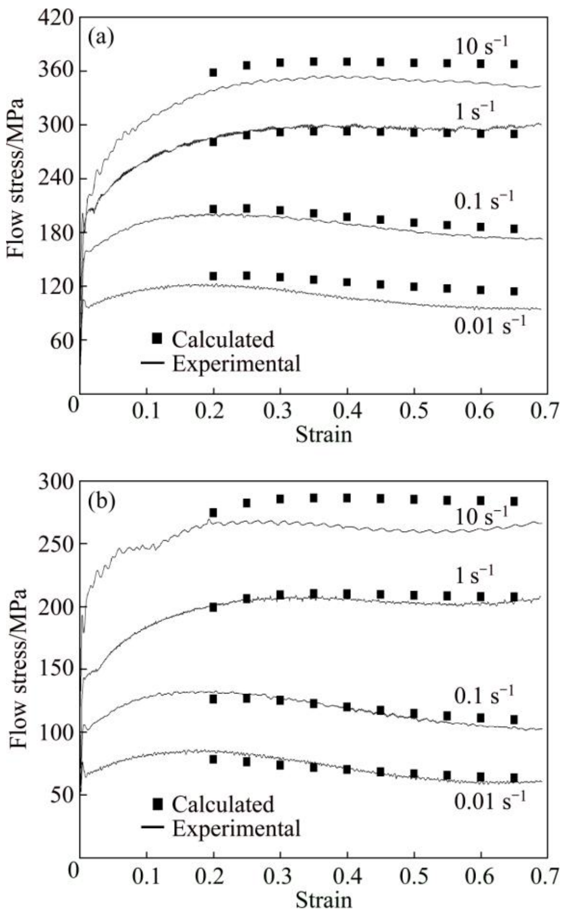

Fig. 10 Comparison of calculated flow stress−strain curves of superalloy GH696 with experimental ones at different deformation temperatures: (a) 1000 ℃; (b) 1090 ℃

The calculated average absolute relative errors are 7.08% and 4.74% at the deformation temperatures of 1000 ℃ and 1090 ℃, respectively. And the total average relative error is 5.91%, which is acceptable in model calculation. This result demonstrates that the proposed constitutive equation provides an accurate and precise estimation of the flow stress of GH696 superalloy.

4 Conclusions

1) The flow stress of superalloy GH696 increases with the increase of strain rate and decreases with the increase of deformation temperature. The flow stress−strain curves represent the occurrence of dynamic recovery at lower deformation temperatures and higher strain rates, and dynamic recrystallization at higher deformation temperatures and lower strain rates.

2) The strain rate sensitivity exponent increases with the increase of deformation temperature and decreases with the increase of strain rate. The strain hardening exponent decreases with the increase of deformation temperature.

3) The apparent activation energy for deformation of superalloy GH696 is in the range of 389.524−410.236 kJ/mol at strains of 0.20−0.60.

4) The model describing the dependence of flow stress of superalloy GH696 on the deformation temperature, strain rate and strain is developed. The total average relative error between the calculated and the experimental flow stress of superalloy GH696 is 5.91%.

References

[1] KUSABIRAKI K, AMADA E, OOKA T. Precipitation and growth of γ' phase in an Fe−38Ni−13Co−4.7Nb superalloy [J]. ISIJ International, 1996, 36(2): 208−214.

[2] KUSABIRAKI K, AMADA E, OOKA T, SAJI S. Epsilon and eta phases precipitated in an Fe−38Ni−13Co−4.7Nb−0.4Si superalloy [J]. ISIJ International, 1997, 37(1): 80−86.

[3] KUSABIRAKI K, TSUJINO H, SAJI S. Effects of tensile stress on the high-temperature oxidation of an Fe−38Ni−13Co−4.7Nb−1.5Ti−0.4Si superalloy in air [J]. ISIJ International, 1998, 38(9): 1015−1021.

[4] CAI D Y, ZHANG C L, TANG Z G, DONG H F, WANG P. Processing maps for Fe−24Ni−11Cr−3Ti−1Mo superalloy [J]. Bulletin Materials Science, 2011, 34(3): 525−529.

[5] DEHGHAN A H, ABBASI S M, MOMENI A, KARIMI TAHERI A. On the constitutive modeling and microstructural evolution of hot compressed A286 iron-base superalloy [J]. Journal of Alloys and Compounds, 2013, 564: 13−19.

[6] de CICCO H, LUPPO M I, RAFFAELI H, DI GAETANO J, GRIBAUDO L M, OVEJERO-GARCÍA J. Creep behavior of an A286 type stainless steel [J]. Material Characterization, 2005, 55: 97−105.

[7] GAO H, BARBER G C, CHEN Q A, LU Y Q. High temperature deformation of a Fe-base low nickel alloy [J]. Journal of Materials Processing Technology, 2003, 142: 52−57.

[8] LI M Q, JU W B, LIN Y Y, WANG X J, NIU Y. Deformation behavior of GH4169 nickel based superalloy in isothermal compression [J]. Materials Science and Technology, 2008, 24(10): 1195−1198.

[9] LI M Q, YAO X Y, LUO J, LIN Y Y, SU S B. Modeling for flow stress of the nickel-based GH4169 superalloy [J]. Acta Metallurgica Sinica, 2007, 43: 937−942.

[10] MEDEIROS S C, PRASAD Y V R K, FRAZIER W G, SRINIVASAN R. Modeling grain size during hot deformation of IN718 [J]. Scripta Materialia, 2000, 42: 7−23.

[11] WU H Y, ZHU F J, WANG S C, WANG W R, WANG C C, CHIU C H. Hot deformation characteristics and strain-dependent constitutive analysis of Inconel 600 superalloy [J]. Journal of Materials Science, 2012, 47: 3971−3981.

[12] NIE L F, ZHANG L W, ZHU Z, XU W. Constitutive modeling of dynamic recrystallization kinetics and processing maps of solution and aging FGH96 superalloy [J]. Journal of Materials Engineering and Performance, 2013, 22: 3728−3734.
[13] LOPEZ B, URCOLA J J. Hot deformation characteristics of Inconel 625 [J]. Materials Science and Technology, 1996, 12: 673−678.
[14] WU K, LIU G Q, HU B F, LI F, ZHANG Y W, TAO Y, LIU J T. Hot compressive deformation behavior of a new hot isostatically pressed Ni−Cr−Co based powder metallurgy superalloy [J]. Materials and Design, 2011, 32: 1872−1879.
[15] ZHANG P, HU C, ZHU Q, DING C G, QIN H Y. Hot compression deformation and constitutive modeling of GH4698 alloy [J]. Materials and Design, 2015, 65: 1153−1160.
[16] LIN Y C, WEN D X, DENG J, LIU G, CHEN J. Constitutive models for high-temperature flow behaviors of a Ni-based superalloy [J]. Materials and Design, 2014, 59: 115−123.
[17] WANG K, LI M Q, LUO J, LI C. Effect of the δ phase on the deformation behavior in isothermal compression of superalloy GH4169 [J]. Materials Science and Engineering A, 2011, 528: 4723−4731.
[18] ABBASI S M, MOMENI A. Hot working behavior of Fe−29Ni−17Co analyzed by mechanical testing and processing map [J]. Materials Science and Engineering A, 2012, 552: 330−335.
[19] SALEHI A R, SERAJZADEH S, YAZDIPOUR N. A study on flow behavior of A-286 superalloy during hot deformation [J]. Materials Chemistry and Physics, 2007, 101: 153−157.
[20] EBRAHIMI R, PARDIS N. Determination of strain-hardening exponent using double compression test [J]. Materials Science and Engineering A, 2009, 518: 56−60.
[21] WU B, LI M Q, MA D W. The flow behavior and constitutive equations in isothermal compression of 7050 aluminum [J]. Materials Science and Engineering A, 2012, 542: 79−87.
[22] STÜWE H P, LES P. Strain rate sensitivity of flow stress at large strains [J]. Acta Materialia, 1998, 46: 6375−6380.
[23] China Areonautical Materials Handbook Editorial Committee. China areonautical materials handbook [M]. 2nd ed. Beijing: Standards Press of China, 1989. (in Chinese)
[24] SELLARS C M, TEGART W J M G. On the mechanism of hot deformation [J]. Acta Metallurgica, 1966, 14: 1136−1138.
[25] YUAN H, LIU W C. Effects of the δ phase on the hot deformation behavior of Inconel 718 [J]. Materials Science and Engineering A, 2005, 408: 281−289.

GH696 合金高温变形过程中的塑性变形行为

许赵华，李淼泉，李 宏

西北工业大学 材料学院，西安 710072

摘 要：为了研究 GH696 合金的热变形行为，在 880~1120 ℃、0.01~10 s^{-1} 条件下对其进行一系列等温压缩试验，所有试样的变形量为 50%。计算各变形条件下的应变速率敏感性指数(m)及应变硬化指数(n)，并分析加工参数对 m 和 n 值的影响。结果表明，流变应力随着应变速率的增大及变形温度的降低而增大。m 值随变形温度的升高而增大，随应变速率的增大而减小，而 n 值则随着变形温度的升高而减小。此外，建立了 GH696 合金热变形过程中的流变应力模型，由模型计算得到的流变应力与实验结果吻合较好。

关键词：GH696 合金；流变应力；变形行为；应变速率敏感性指数；应变硬化指数；流变应力模型

(Edited by Wei-ping CHEN)